Multiscale Modeling of Calcium Dynamics in Ventricular Myocytes With Realistic Transverse Tubules

Zeyun Yu*, Guangming Yao, Masahiko Hoshijima, Anushka Michailova, and Michael Holst

***Abstract*—Spatial-temporal Ca^{2+} dynamics due to Ca^{2+} release, buffering, and reuptaking plays a central role in studying excitation–contraction (E–C) coupling in both normal and diseased cardiac myocytes. In this paper, we employ two numerical methods, namely, the meshless method and the finite element method, to model such Ca^{2+} behaviors by solving a nonlinear system of reaction–diffusion partial differential equations at two scales. In particular, a subcellular model containing several realistic transverse tubules (or t-tubules) is investigated and assumed to reside at different locations relative to the cell membrane. To this end, the Ca^{2+} concentration calculated from the whole-cell modeling is adopted as part of the boundary constraint in the subcellular model. The preliminary simulations show that Ca^{2+} concentration changes in ventricular myocytes are mainly influenced by calcium release from t-tubules.**

***Index Terms*—Calcium dynamics, finite element methods (FEMs), meshless methods, numerical simulation, ventricular myocytes.**

I. Introduction

THE HIGH prevalence of heart failure is largely due to our lack of accurate understanding of the complex pathology including abnormal excitation–contraction (E–C) coupling in cardiomyocytes. The architecture of uniquely developed membrane organelles in ventricular myocytes, including transverse tubules (t-tubules) and junctional sarcoplasmic reticulum (jSR), and the arrangement of associated proteins are known to play a major role in dynamically controlling intracellular Ca^{2+} levels, which in turn regulate cardiac contraction and other cellular functions [1]. For its central role in E–C coupling, modeling Ca^{2+} release, and concentration change has been an active research area and is typically studied in two ways: stochastic approaches that employ Monte Carlo simulation [2] and deterministic approaches based on partial differential equations (PDEs) [3]. While stochastic simulation at the nanometer scale provides elementary information on Ca^{2+} dynamics, cardiac cell contraction is most closely related to the intracellular Ca^{2+} concentration level $[Ca^{2+}]_i$ [4]. For this reason, our interest in this paper is to investigate spatial-temporal variations of intracellular Ca^{2+} concentration at cellular and subcellular levels, where the stochastic behavior of Ca^{2+} dynamics is so insignificant that deterministic methods utilizing PDEs are more appropriate.

Most of the previous work using PDEs to study Ca^{2+} dynamics was conducted based on idealized geometries such as cylindrical shapes [3], [5]. As pointed out in [2] and [3], geometric changes may significantly influence the behaviors of Ca^{2+} dynamics both locally and globally. For example, the heart failure is closely related to rearrangement or lack of t-tubules in cardiac cells [6], [7]. In fact, a recent study by Cheng *et al.* [8], which utilizes a single t-tubular branch generated from light microscopic images, suggests that the quantitative understanding of Ca^{2+} signaling requires more accurate knowledge of t-tubular ultrastructures. Thus, one of the focuses in this paper is to include nanometer-scale, realistic surface geometries of multiple t-tubules that are constructed from 3-D electron microscopic (EM) images of the ventricular myocytes of an adult mouse [9]. It is worth noting that in mice both transverse tubules and axial tubules are found and often known as transverse-axial tubules (or TATs) [10]. However, t-tubular branches are naturally more frequently observed than axial tubules. In addition, the 3-D EM tomographic data we have used for the current study are so thin that there is no obvious axial tubule in the image. Therefore, we shall still adopt the name "t-tubule" instead of "TAT" throughout this paper.

The underlying PDEs describing Ca^{2+} dynamics in ventricular myocytes may be numerically solved by such techniques as the finite difference method (FDM) [11], the finite element method (FEM) [12], [13], the finite volume method [14], and the boundary element method [15]. All these methods are mesh based, meaning that meshes or grids must be constructed on the problem domain. Another numerical approach known as the meshless method [16] does not require explicit meshes and,

Manuscript received April 11, 2011; revised May 18, 2011; accepted May 20, 2011. Date of publication May 31, 2011; date of current version September 21, 2011. This work was supported in part by the NIH Award Number R15HL103497 from the National Heart, Lung, and Blood Institute, the National Biomedical Computation Resource NIH Award Number P41 RR08605, and the UWM Research Growth Initiative. M. Hoshijima is partly supported by American Heart Association under 0840013N. *Asterisk indicates corresponding author*.

*Z. Yu is with the Department of Computer Science, University of Wisconsin-Milwaukee, Milwaukee, WI 53211 USA (e-mail: yuz@uwm.edu).

G. Yao is with the Department of Computer Science, University of Wisconsin-Milwaukee, Milwaukee, WI 53211 USA (e-mail: guangmingyao@gmail.com).

M. Hoshijima is with the Department of Medicine, University of California-San Diego, CA 92093 USA (e-mail: mhoshijima@ucsd.edu).

A. Michailova is with the Department of Bioengineering, University of California-San Diego, CA 92093 USA (e-mail: amihaylo@bioeng.ucsd.edu).

M. Holst is with the Departments of Mathematics and Physics, University of California-San Diego, CA 92093 USA (e-mail: mholst@math.ucsd.edu).

Color versions of one or more of the figures in this paper are available online at http://ieeexplore.ieee.org.

Digital Object Identifier 10.1109/TBME.2011.2158316

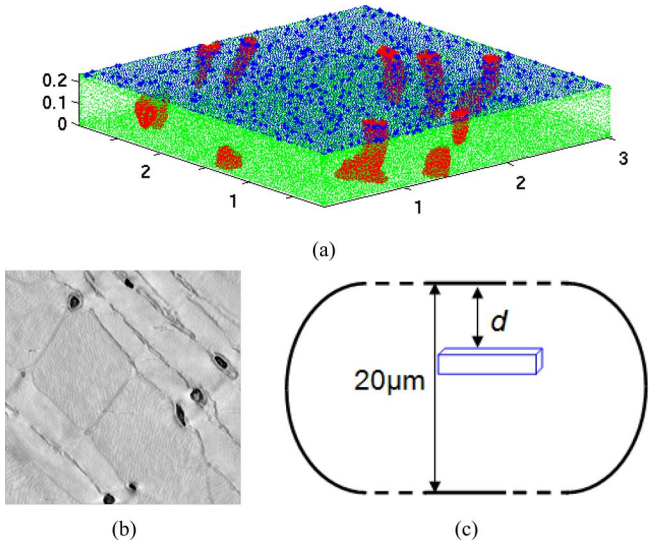

Fig. 1. (a) Multiple t-tubule geometry and its surrounding box domain, denoted by Ω. The red color in Ω represents t-tubules (denoted by Γ_1), the top blue face of the box (denoted by Γ_2) satisfies the Dirichlet boundary condition, and a reflective boundary condition is assumed on the remaining boundary faces (in green). (b) One slice of the 3-D electron tomographic map, showing t-tubules in dark regions surrounded by jSR. (c) Model in (a) is placed at various locations in a simplified whole-cell model at a distance d ($d =$, 2, or 0 μm) from the cell membrane.

thus, has gradually become popular in the past two decades. Our recent work (unpublished) has shown that this method can be easily adapted to handle very large systems. However, numerically it is not as stable as the FEM. For these reasons, in this study, we employ both meshless and FEMs to study Ca^{2+} dynamics at different scales.

II. Geometric and Mathematical Modeling

A. Geometric Model

Fig. 1(a) shows the geometric model containing several t-tubules extracted from the ventricular myocytes of an adult mouse. The details of EM imaging and 3-D tomographic reconstruction can be found in [9]. The algorithmic details of image processing and boundary segmentation are described in [17]. Fig. 1(b) shows one slice of the reconstructed tomographic map, where dark regions are t-tubules surrounded by jSR (not considered in this study). The rectangle-shaped model in Fig. 1(a), denoted by $\Omega \subset \mathbb{R}^3$, is the problem domain in our simulations and the dimension of the box is measured $2.81\,\mu\text{m} \times 2.79\,\mu\text{m} \times 0.24\,\mu\text{m}$. The boundary Γ_1 (in red) represents realistic t-tubules and Γ_2 (in blue) is the top face of Ω. Because the location of the constructed t-tubules in the ventricular myocyte is unknown and we are also interested in the roles of t-tubules and cell membrane in calcium dynamics, we shall consider three cases in our simulations by placing the model in Fig. 1(a) in a simplified whole-cell model such that the top face Γ_2 is at a distance d ($d = 8$, 2, or 0 μm) away from the cell membrane [see Fig. 1(c)].

B. Governing Equations

The following nonlinear reaction–diffusion equations, defined on the model described earlier, are modified from [18]

$$\begin{aligned}
\frac{\partial[\mathrm{Ca}^{2+}]_i}{\partial t} &= D_{Ca}\nabla^2[\mathrm{Ca}^{2+}]_i - \sum_{m=1}^{3} R_{Bm} - R_{Bs},\ \Omega \\
\frac{\partial[CaB_m]}{\partial t} &= D_{CaBm}\nabla^2[CaB_m] + R_{Bm}, m = 1,2,3,\ \Omega \\
\frac{\partial[CaB_s]}{\partial t} &= R_{B_s},\ \Omega \\
\frac{\partial[\mathrm{Ca}^{2+}]_i}{\partial t} &= D_{Ca}\nabla^2[\mathrm{Ca}^{2+}]_i + J_{Ca\mathrm{flux}},\ \Gamma_1 \\
[\mathrm{Ca}^{2+}]_i &= [\mathrm{Ca}^{2+}]_{i_0}, \Gamma_2
\end{aligned} \tag{1}$$

with the following initial conditions:

$$\begin{aligned}
&[\mathrm{Ca}^{2+}]_i = 0.10\,\mu\text{M},\ [CaB_1] = 11.92\,\mu\text{M} \\
&[CaB_2] = 0.97\,\mu\text{M},\ [CaB_3] = 0.13\,\mu\text{M} \\
&[CaB_s] = 6.36\,\mu\text{M}.
\end{aligned}$$

The boundary Γ_2 [the top face in Fig. 1(a)] satisfies the Dirichlet boundary condition, and a reflective boundary condition is assumed on the remaining faces of the box. The Ca^{2+} concentration, $[\mathrm{Ca}^{2+}]_{i_0}$, on Γ_2 is obtained from the whole-cell modeling using the messless method (see later).

In our model, three types of mobile Ca^{2+} buffers (Fluo-3, ATP, and calmodulin, denoted by B_m, $m = 1, 2, 3$, respectively), and one type of stationary Ca^{2+} buffers (troponin, denoted by B_s) are considered. Their concentrations are denoted by $[\mathrm{Ca}^{2+}]_i, [CaB_m], m = 1, 2, 3, [CaB_s]$, respectively. The reactions between Ca^{2+} ions and buffers are defined as follows:

$$R_{Bm} = k_+^m\left([B_m] - [CaB_m]\right)[\mathrm{Ca}^{2+}]_i - k_-^m[CaB_m] \tag{2}$$

$$R_{Bs} = k_+^m\left([B_s] - [CaB_s]\right)[\mathrm{Ca}^{2+}]_i - k_-^m[CaB_s] \tag{3}$$

where $m = 1, 2, 3$.

At the resting (initial) state, we assume uniform distributions of all the buffers throughout the cytosol. The resting concentrations of mobile and stationary buffers satisfy equilibrium conditions (i.e., $R_{Bm} = R_{Bs} = 0$) [19] with the resting Ca^{2+} concentration at $0.1\,\mu$M. The total Ca^{2+} flux, $J_{Ca\mathrm{flux}}$, on the t-tubule surface is defined as in [18]

$$J_{Ca\mathrm{flux}} = J_{Ca} + J_{NCX} - J_{pCa} + J_{Cab} \tag{4}$$

where calcium influx/efflux through L-type calcium channels LCCs, J_{Ca}, sodium–calcium exchangers NCXs, J_{NCX}, calcium pump efflux J_{pCa}, and calcium background leak influx J_{Cab} are included. The current densities, I_{Ca}, I_{NCX}, I_{pCa}, and I_{Cab}, are calculated the same as in [18]. The physical constants and parameters are taken from [18] and [20]. To calculate the total Ca^{2+} flux, $J_{Ca\mathrm{flux}}$, each of the current densities is converted into Ca^{2+} flux by using

$$J_i = \beta_i \frac{V_{mc}}{S_{mc}}\left(\frac{1}{2F}\frac{C_m}{V_{\mathrm{cell}}}\right) I_i \tag{5}$$

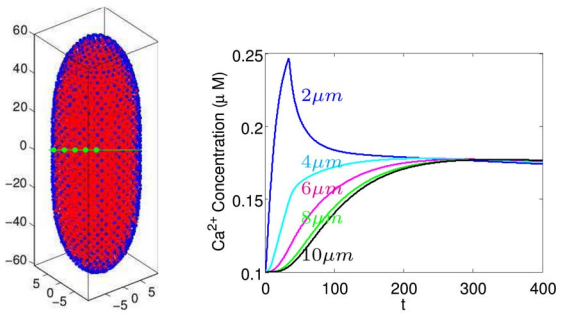

(a) (b)

Fig. 2. (a) Whole-cell model of approximately $120\,\mu\text{m} \times 20\,\mu\text{m} \times 20\,\mu\text{m}$, with t-tubules and all intracellular structures excluded. Indicated in green is a scanning line going through the center of the cell, with five feature spots that are 2, 4, 6, 8, and $10\,\mu$m away from the cell membrane. (b) Local Ca^{2+} transients taken at the five feature spots shown in (a).

with $i = Ca, NCX, pCa$, or Cab. The capacitance to rendered volume ratio (C_m/V_{cell}) is assumed to be $8.8pF/pL$ [21]. Note that S_{mc} is the total area of t-tubule membrane where Ca^{2+}-related channels reside and V_{mc} is the volume of the model. In Fig. 1(a), $V_{mc} = 1.782\,\mu\text{m}^3$, and $S_{mc} = 0.919\,\mu\text{m}^2$. The model-dependent scaling parameter, $\beta_{Ca} = 4.0$, and $\beta_{NCX} = \beta_{pCa} = \beta_{Cab} = 1.0$. The voltage clamp protocol is assumed to hold the potential -50 mV with an electric pulse of 10 mV for 70 ms [18].

III. Methodology

To solve the system of equations in (1), we use an explicit time-stepping method in time and the FEM in space. Since we consider Γ_2 at different locations in a simplified ventricular myocyte, predicting the initial Ca^{2+} concentration, $[\text{Ca}^{2+}]_{i_0}$, on Γ_2 is necessary and is performed by using the meshless method.

A. Meshless Method

A simplified whole-cell model, as shown in Fig. 2(a), is considered. To predict spatial-temporal Ca^{2+} concentrations in a large domain, the meshless method is a good choice compared with other numerical methods, for its implementation simplicity, time efficiency, and effectiveness in dealing with complicated geometries [22]. In particular, the FDM has been utilized in [5] for whole-cell calcium modeling, but the meshless method can handle smooth yet complex domain boundaries more effectively. In our meshless method, the operator-splitting method is used to decouple the PDEs and to separate nonlinear sources and the Laplacian operators. The local radial basis function collocation method (LRBFCM) [16] is employed to approximate Laplacian terms at every time step. With the predicted spatial-temporal Ca^{2+} concentrations, Fig. 2(b) shows local Ca^{2+} transients at five representative spots that are 2, 4, 6, 8, and $10\,\mu$m away from the cell membrane. For the subcellular modeling problem [see Fig. 1(a)], we consider three locations [see Fig. 1(c)], where $d = 0\ \mu\text{m}, 2\ \mu\text{m}, 8\ \mu\text{m}$. The concentrations at these locations in the whole-cell modeling shall be used later as the boundary condition for Γ_2 in the system (1).

B. FEM

With the initial concentration $[\text{Ca}^{2+}]_{i_0}$ predicted on Γ_2, we employ the finite element toolkit FETK (http://FETK.org) and the CSMOL software (http://mccammon.ucsd.edu/smol/) [23] to solve the system (1) on the geometric model shown in Fig. 1(a). The software toolkit called GAMer [24] is used to discretize the complex domain into a tetrahedral mesh. In the present simulation, we have $83\,614$ nodes (vertices) and $350\,249$ tetrahedra. The time-step size is chosen as 4 ms. It takes about 55 min to compute the concentrations for a time period of $[0, 400\,\text{ms}]$ on a single Intel Xeon-based processor (3.00 GHz). The numerical results next are visualized by Meshlab and MATLAB 2.7.7.

IV. Results

In this study, the SR has been excluded from the finite element simulations shown later. Fig. 3 shows the results with the presence of $100\,\mu$M Fluo-3, where the geometric model used is given in Fig. 1(a). The global and local Ca^{2+} transients reach the peaks at about 72 ms when the LCC current is completely blocked. Fig. 3(a) and (b) shows the voltage-clamp protocol and the whole-cell L-type Ca^{2+} current as used in [18].

In Fig. 3(c)–(l), we show three boundary conditions on Γ_2, where Γ_2 is assumed to be $8\,\mu$m (blue lines), $2\,\mu$m (green lines), and $0\,\mu$m (red lines) away from the cell membrane [see Fig. 1(c)]. Fig. 3(c)–(e) shows the averaged current densities of $\text{Na}^+/\text{Ca}^{2+}$ exchangers, Ca^{2+} pumps, and Ca^{2+} leaks, assuming a uniform distribution of Ca^{2+} inside the model. Fig. 3(f) shows the averaged Ca^{2+} concentration over time. The time-varying concentrations of the calcium-bound mobile and stationary buffers are shown in Fig. 3(g)–(j). In the presence of LCC current densities, these concentrations rapidly increase. After the LCC current is blocked, the concentrations of the calcium-bound buffers gradually decrease and become stable when the free Ca^{2+} concentration is stable. In all these results, the curves are almost identical in the two conditions where Γ_2 is 8 and $2\,\mu$m away from the cell membrane, suggesting that the main contribution to calcium concentration changes in ventricular myocytes comes from t-tubules except in the regions near the cell membrane.

While the averaged Ca^{2+} concentration within the cytosol of the model is shown in Fig. 3(f), we also consider two feature spots along a scanning line going vertically through the center of the box in Fig. 1(a). These two spots are 0.235 and $0.0038\,\mu$m away from the top surface Γ_2 of the box, and the calcium concentration changes over time are given in Fig. 3 (k) and (l), respectively. Again, when the model is placed near the cell membrane, we observe significantly higher Ca^{2+} concentration than the other two cases. When the feature spot is chosen near the top surface Γ_2, the other two cases [green and blue lines in Fig. 3(l)] are also distinguishable.

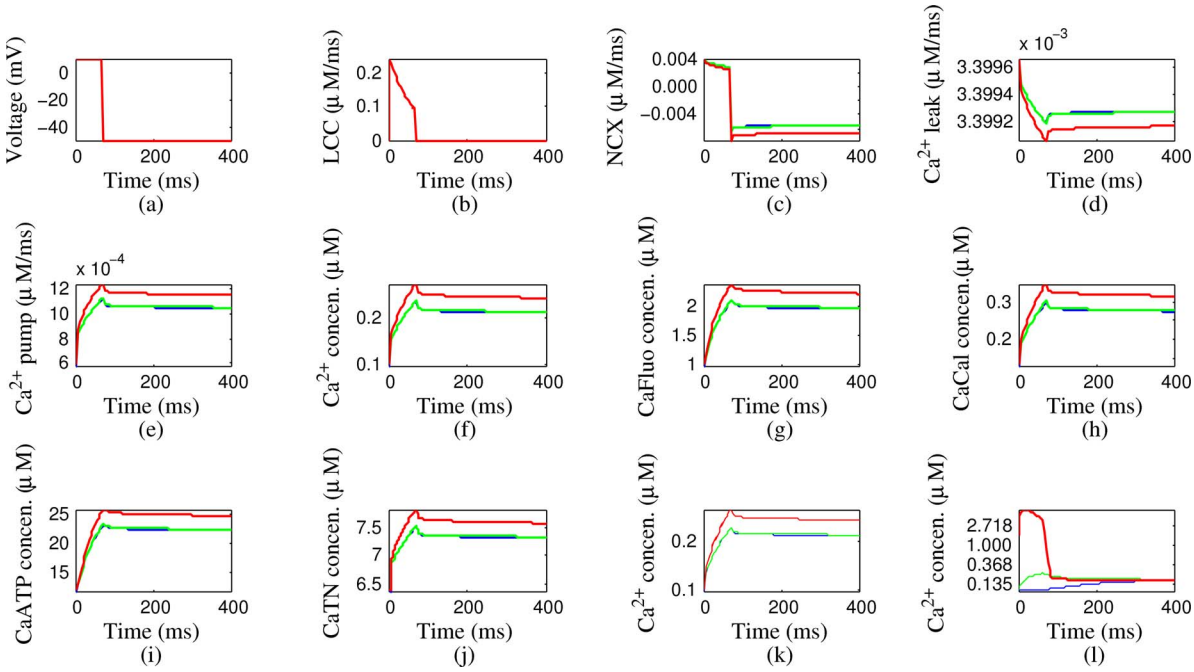

Fig. 3. Calcium signaling simulations with realistic t-tubule membrane. The upper boundary Γ_2 of the subcellular model [see Fig. 1(a)] is assumed to be $8\,\mu$m (blue lines), $2\,\mu$m (green lines), and $0\,\mu$m (red lines) away from the cell membrane (also see Fig. 1). Note that in most of the simulations plotted here, the blue lines are almost identical to the green lines. (a) and (b) Voltage-clamp protocol and the whole-cell LCC current used in the simulation. (c) and (f) Predicted global Na^+/Ca^{2+}, Ca^{2+} pump and leak currents and global average Ca^{2+} transient when Ca^{2+} is uniformly distributed inside the cell. (g) and (j) Predicted average concentrations of calcium-bound mobile and stationary buffers. (k) and (l) Local Ca^{2+} transients taken at two feature spots that are $0.235\,\mu$m (k) and $0.0038\,\mu$m (l) away from Γ_2.

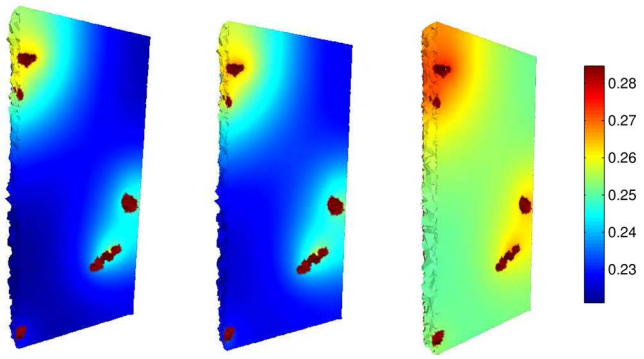

Fig. 4. 3-D views of the Ca^{2+} concentrations at the $[Ca^{2+}]_i$ peak of 72 ms when the subcellular model in Fig. 1(a) is placed $8\,\mu$m (left), $2\,\mu$m (middle), and $0\,\mu$m (right) away from the cell membrane. Note that the left portion (about one half) of the domain has been cutout.

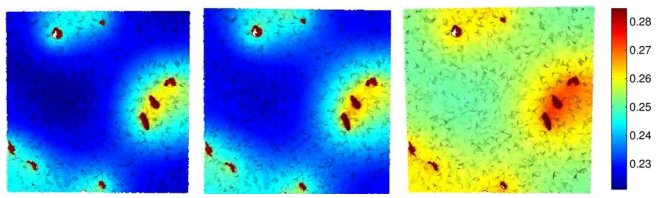

Fig. 5. Cross-sectional views of the Ca^{2+} concentrations at the $[Ca^{2+}]_i$ peak of 72 ms when the subcellular model in Fig. 1(a) is placed $8\,\mu$m (left), $2\,\mu$m (middle), and $0\,\mu$m (right) away from the cell membrane. About a half of the domain has been cutout in the front to show the cross-sectional views.

The model is able to predicate local Ca^{2+} transient peaks at approximately 72 ms. Fig. 4 and Fig. 5 shows the 3-D local Ca^{2+} transients when $t = 72$ ms. The local Ca^{2+} transients near the t-tubular surface are about 10%–20% higher than elsewhere. When the distance from the cell membrane to Γ_2 increases (i.e., going from 0, 2 to $8\,\mu$m), the Ca^{2+} concentration undergoes a quick ($\sim 15\%$) decrease and then becomes stable, as also seen in [8], suggesting that the influence from the surface membrane rapidly diminishes. The difference between the bulk and subsarcolemmal Ca^{2+} concentrations had been discussed in previous studies (i.e., [25]). Another factor of the Ca^{2+} concentration changes observed in Figs. 4 and 5 might be due to the lack of calcium release from SR in this study.

V. Conclusion

In this paper, we employed the FEM and realistic EM structures of t-tubules to investigate calcium dynamics involving calcium releasing, buffering, and reuptaking at the subcellular scale. Different boundary conditions are imposed on the subcellular model by placing the model at three different locations relative to the cell membrane of a simplified ventricular myocyte. The boundary values are borrowed from the whole-cell simulations precomputed by using the meshless method. The preliminary results show that t-tubules, as compared to the cell surface membrane, play a major role in regulating Ca^{2+} concentration changes in ventricular myocytes.

REFERENCES

[1] D. M. Bers, "Calcium cycling and signaling in cardiac myocytes," *Annu. Rev. Physiol.*, vol. 70, pp. 23–49, 2008.

[2] X. Koh, B. Srinivasan, H. S. Ching, and A. Levchenko, "A 3D Monte Carlo analysis of the role of dyadic space geometry in spark generation," *Biophys. J.*, vol. 90, pp. 1999–2014, 2006.

[3] L. T. Izu, S. A. Means, J. N. Shadid, Y. Chen-Izu, and C. W. Balke, "Interplay of ryanodine receptor distribution and calcium dynamics," *Biophys. J.*, vol. 91, pp. 95–112, 2006.

[4] D. M. Bers, "Cardiac excitation-contraction coupling," *Nature*, vol. 415, no. 10, pp. 198–205, 2002.

[5] A. Michailova, F. DelPrincipe, M. Egger, and E. Niggli, "Spatiotemporal features of Ca2+ buffering and diffusion in atrial cardiac myocytes with inhibited sarcoplasmic reticulum," *Biophys. J.*, vol. 83, pp. 3134–3151, 2002.

[6] F. Brette and C. Orchard, "T-tubule function in mammalian cardiac myocytes," *Circulat. Res.*, vol. 92, pp. 1182–1192, 2003.

[7] C. Orchard, M. Pasek, and F. Brette, "The role of mammalian cardiac t-tubules in excitation-contraction coupling: Experimental and computational approaches," *Exp. Physiol.*, vol. 94, pp. 509–519, 2009.

[8] Y. Cheng, Z. Yu, M. Hoshijima, M. Holst, A. McCulloch, J. A. McCammon, and A. P. Michailova, "Numerical analysis of Ca^{2+} signaling in rat ventricular myocytes with realistic transverse-axial tubular geometry and inhibited sarcoplasmic reticulum," *PLoS Comput. Biol.*, vol. 6, no. 10, pp. e1000972 (1–16), 2010.

[9] T. Hayashi, M. E. Martone, Z. Yu, A. Thor, M. Doi, M. Holst, M. H. Ellisman, and M. Hoshijima, "Three-dimensional reconstruction reveals new details of membrane systems for calcium signaling in the heart," *J. Cell Sci.*, vol. 122, pp. 1005–1013, 2009.

[10] M. S. Forbes, L. A. Hawkey, and N. Sperelakis, "The transverse-axial tubular system (TATS) of mouse myocardium: Its morphology in the developing and adult animal," *Amer. J. Anat.*, vol. 170, no. 2, pp. 143–162, 1984.

[11] L. Wu and Y. Kwok, "A front-fixing finite difference method for the evaluation of american options," *Comput. Math. Appl.*, vol. 6, pp. 83–83, 1997.

[12] D. Braess, *Finite Elements. Theory, Fast Solvers and Applications in Solid Mechanics*. Cambridge, U.K.: Cambridge Univ. Press, 2001.

[13] J. Melenk and I. Babuska, "The partition of unity finite element method: Basic theory and applications," *Comput. Meths. Appl. Mech. Engrg.*, vol. 139, pp. 289–314, 1996.

[14] R. Eymard, T. Gallouet, and R. Herbin, "Finite volume methods," in *Techniques of Scientific Computing, Part III, Handbook of Numerical Analysis, VII*, P. G. Ciarlet and J. L. Lions, Eds. Eds. Amsterdam, The Netherlands, North Holland, 2000, pp. 713–1020.

[15] R. Schaback, "Convergence analysis of methods for solving general equations," in *Boundary Elements XXVII*, A. kassab, C. Brebbia, E. Divo, and D. Poljak, Eds. Southampton, U.K.: WIT Press, 2005, pp. 17–24.

[16] B. Šarler and R. Vertnik, "Meshfree explicit local radial basis function collocation method for diffusion problems," *Comput. Math. Appl.*, vol. 51, pp. 1269–1282, 2006.

[17] Z. Yu, M. Holst, T. Hayashi, C. L. Bajaj, M. H. Ellisman, J. A. McCammon, and M. Hoshijima, "Three-dimensional geometric modeling of membrane-bound organelles in ventricular myocytes," *J. Struct. Biol.*, vol. 164, no. 3, pp. 304–313, 2008.

[18] S. Lu, A. Michailova, J. Saucerman, Y. Cheng, Z. Yu, T. Kaiser, W. Li, R. Bank, M. Holst, J. Mccammon, T. Hayashi, M. Hoshijima, P. Arzberger, and A. McCulloch, "Multiscale modeling in rodent ventricular myocytes," *IEEE Eng. Med. Biol. Mag.*, vol. 28, no. 2, pp. 46–57, Mar. 2009.

[19] V. Matveev, R. S. Zucker, and A. Sherman, "Facilitation through buffer saturation: Constraints on endogenous buffering properties," *Biophys. J.*, vol. 86, no. 5, pp. 2691–2709, 2003.

[20] R. Hinch, J. Greenstein, A. Tanskanen, L. Xu, and R. Winslow, "A simplified local control model of calcium-induced calcium release in cardiac ventricular myocytes," *Biophys. J.*, vol. 87, no. 6, pp. 3723–3736, 2004.

[21] H. Satoh, L. Delbridge, L. Blatter, and D. Bers, "Surface: Volume relationship in cardiac myocytes studied with confocal microscopy and membrane capacitance measurements: Species-dependence and developmental effects," *Biophys. J.*, vol. 70, no. 3, pp. 1494–1504, 1996.

[22] A. Karageorghis, C. S. Chen, and Y.-S. Smyrlis, "Matrix decomposition rbf algorithm for solving 3D elliptic problems," *Eng. Anal. Boundary Elements*, vol. 33, pp. 1368–1373, 2009.

[23] Y. H. Cheng, J. K. Suen, D. Q. Zhang, S. D. Bond, Y. J. Zhang, Y. H. Song, N. A. Baker, C. L. Bajaj, M. J. Holst, and J. A. McCammon, "Finiteelement analysis of the time-dependent smoluchowski equation for acetylcholinesterase reaction rate calculations," *Biophys. J.*, vol. 92, pp. 3397–3406, 2007.

[24] Z. Yu, M. Holst, and J. A. McCammon, "High-fidelity geometric modelling for biomedical applications," *Finite Elements Anal. Design*, vol. 44, pp. 715–723, 2008.

[25] A. W. Trafford, M. E. Diaz, S. C. O'Neill, and D. A. Eisner, "Comparison of subsarcolemmal and bulk calcium concentration during spontaneous calcium release in rat ventricular myocytes," *J. Physiol.*, vol. 488, pp. 577–586, 1995.